Materialia 6 (2019) 100299

Contents lists available at ScienceDirect

Materialia

journal homepage: www.elsevier.com/locate/mtla

Transformation-induced plasticity and high strength in beta titanium alloy manufactured by selective laser melting

Y.J. Liu[a], Y.S. Zhang[b,*], L.C. Zhang[a,*]

[a] School of Engineering, Edith Cowan University, 270 Joondalup Drive, Joondalup, Perth, WA 6027, Australia
[b] Northwest Institute for Nonferrous Metal Research, Xi'an 710016, China

ARTICLE INFO

Keywords:
Selective laser melting
Beta titanium
Trip effect
Microstructure
Plasticity

ABSTRACT

This work reports simultaneous achievement of high strength and large tensile ductility in a beta titanium alloy manufactured by selective laser melting (SLM). The SLM-produced samples present a unique microstructure and great mechanical behavior due to fast cooling in SLM process. Simultaneous improvement in yield strength (~592±21 MPa), ultimate tensile strength (716±14 MPa) and ductility (37±5%) of SLM-produced sample results from the combination of fine columnar grains and sub-grains, strong texture and the transformation-induced plasticity (TRIP) and "hard-wraps-soft" effects. The large amount of sub-grain boundaries and strong texture delay the initiation of martensitic transformation in the SLM-produced sample, thereby increasing its yield strength.

Titanium alloys have been widely used in biomedical industries thanks to their great mechanical properties and good corrosion resistance [1–5]. Recently, metastable β-type titanium alloys are reported to exhibit low elastic modulus, shape memory property, superelasticity, high biocompatibility and excellent corrosion resistance; therefore they have been received considerable attention as biomedical alloys [6–9]. Several metastable β titanium alloys have been developed in Ti-Nb, Ti-Nb-Ta, Ti-Nb-Sn, Ti-Nb-Ta-Zr alloys for biomedical applications, but most of them still exhibit low strength, low ductility or higher elastic modulus, which makes them unfavorable for hard tissues implants [7,9–12]. Thus, it is challenging to develop a β titanium (and other metallic materials as well) that simultaneously exhibits a high strength and a large ductility. Interestingly, TLM alloy (Ti-25Nb-3Zr-3Mo-2Sn) was reported to possess high strength and low elastic modulus and hot rolling can increase its ductility by scarifying its strength but without changing its elastic modulus due to the transformation-induced plasticity (TRIP) effect and/or the well-known intrinsic trade-off relationship between strength and ductility [13].

It is well know that the mechanical properties of an alloy are sensitive to its microstructural characteristics in terms of phase constituents, phase/grain size and orientation (i.e. texture) [14]. Usually, grain refinement for bulk samples is realized through plastic deformation techniques such as rolling, drawing, forging, equal channel angular pressing (ECAP), and so on [15–17]. The formation of, and interactions among, sub-boundaries or transformation of crystal orientations are commonly reported in the process of plastic deformation [18]. However, these traditional methods have difficulty to refine grains for the samples with complex shape. As one of common metal additive manufacturing technologies, selective laser melting (SLM) has received increasing attention owing to its capability of manufacturing complex parts with near-full relative density and excellent mechanical properties [19]. More importantly, besides sub-grains, strong texture, nano-sized segregation and much finer microstructure are formed in SLM-produced parts compared to their cast and/or rolled counterparts as a result of the high cooling rate [7,14]. This indicates that SLM can refine grain size for both solid and porous samples. Some metastable β titanium parts in solid and porous structures have been produced by SLM, and their fracture mechanisms were studied in relation with the processing parameters and the resultant microstructure (in terms of grain size or texture) [20–22]. For example, Zhang et al. [6] revealed that both the hardness and tensile properties of SLM-produced β Ti-24Nb-4Zr-8Sn components are enhanced by optimal laser scan speed. Interestingly, the samples with the same relative density but produced at different scan speeds display different ductility. This is mainly caused by the difference in microstructure, resulted from the different processing parameters and the cooling rates in SLM process. Such a unique microstructure created in the SLM-produced β titanium parts would affect their mechanical properties. Yang et al. [23] reported that the good ductility of SLM-produced β titanium parts is attributed to the effect of "hard-wraps-soft" structure caused by the melt pool boundaries. However, TRIP effects has not been considered in these cases, and there is no study on the TRIP effect in SLM-produced metastable β titanium parts. Actually, the deformation

* Corresponding authors.
E-mail addresses: y.sh.zhang@c-nin.com (Y.S. Zhang), l.zhang@ecu.edu.au, lczhangimr@gmail.com (L.C. Zhang).

https://doi.org/10.1016/j.mtla.2019.100299
Received 6 February 2019; Accepted 21 March 2019
Available online 26 March 2019

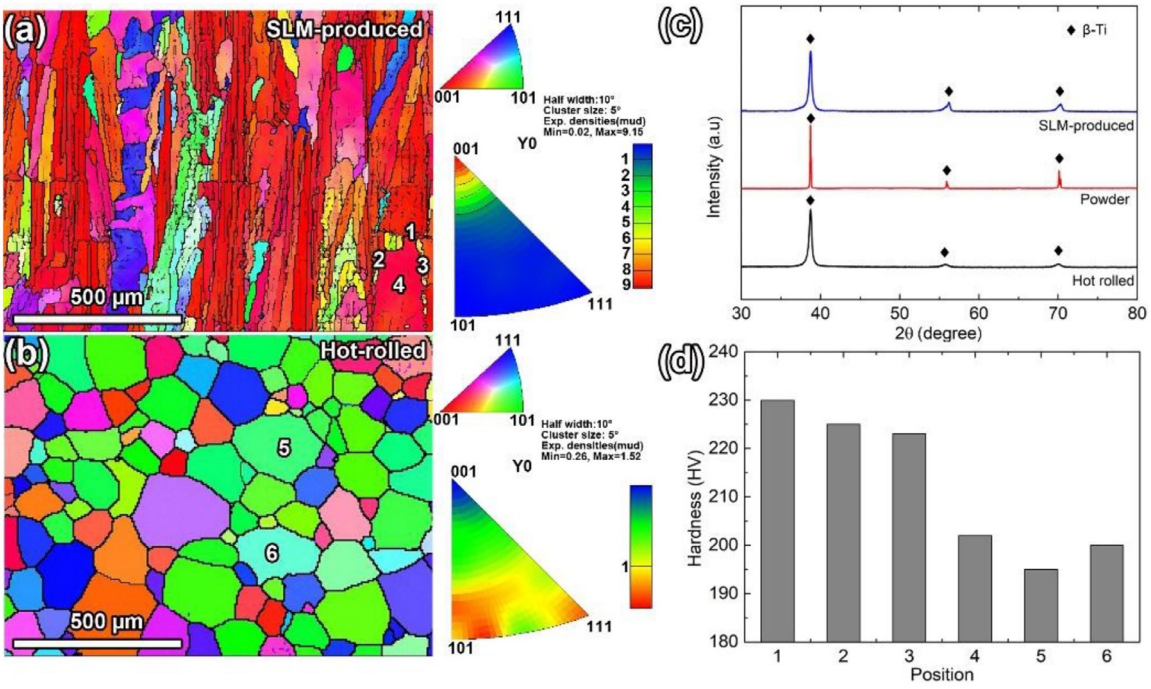

Fig. 1. (a) EBSD mapping of SLM-produced TLM sample on the X–Z cross-section along Z-direction, where a strong texture can be found in inverse pole figure (IPF), (b) EBSD mapping of hot-rolled TLM sample, (c) XRD patterns for the TLM powder used, SLM-produced and hot-rolled samples. All the samples mainly consist of a single β phase, (d) the hardness value at the points 1–6 in the (a) and (b) for SLM-produced and hot-rolled TLM samples.

process in SLM-produced metastable β titanium parts is more complicated than in the conventional parts. As such, this work concentrates on the comparison between SLM-produced and hot-rolled TLM parts in terms of the microstructures and tensile properties to shed light into simultaneous improvement in strength and ductility of SLM-produced TLM sample.

The TLM alloy (Ti-25Nb-3Zr-3Mo-2Sn) powder used in this work was gas atomized and with analyzed chemical composition of 24.98Nb, 2.92Zr, 2.92Mo, 1.86Sn, 0.010 N, 0.0028H, 0.12O, and Ti balance (wt.%). The size of spherical powder ranged between 30 μm and 55 μm with a Gaussian distribution centered ($d_{0.5}$) on about 42 μm. Rectangular TLM samples with size of $80 \times 10 \times 10\ mm^3$ were produced using a BLT-S300 SLM machine with the following optimized processing parameters: input laser power of 300 W, laser scanning speed of 1000 mm/s and layer thickness of 50 μm. The scanning strategy with a zigzag pattern was used to reduce thermal stress in SLM-produced parts. For comparison purpose, hot-rolled samples, which were prepared from a TLM ingot with the rolling temperature of 800 °C followed by a water quenching, were used because of their great combination of mechanical properties [24]. The tensile bars were prepared by wire cutting from the SLM-produced rectangular and hot-rolled bulk samples. The loading direction of SLM-produced tensile bar was along the X axis (the build direction was Z axis), and the loading direction of hot-rolled tensile bar was along the rolling direction. Phase identifications of the samples in as-received condition (i.e. before tensile testing) and after tensile testing were examined using a Panalytical Empyrean X-ray diffractometer (XRD) with Cu Kα radiation ($\lambda = 1.5406$ nm). The microstructural characterization and chemical composition were conducted on Olympus PMG-3 Optical microscope (OM), JSM-6301F field emission scanning electron microscope (SEM) and JEOL-2100 transmission electron microscope (TEM; 200 kV). SEM-based electron back scatter diffraction (EBSD) analyses were conducted in the above mentioned SEM equipped with an Aztec EBSD system with a step size of 0.5 μm. The samples for OM and SEM microstructural observations were etched by a reagent composed of 5% HF, 10% HNO_3, and 85% H_2O (vol.%) for 10 s. The TEM sample was made from the plastic deformation zone near the fracture surface for both samples. The EBSD samples were produced only by grinding and electrolytic polishing. The tensile tests were carried out using an Instron 5869 machine at a strain rate of 0.5 mm/min. The reported tensile properties were averaged from three individual samples.

Fig. 1a and b shows the EBSD inverse pole figure (IPF) result of the SLM-produced TLM sample on the X–Z cross-section along the Z-direction (i.e. the building direction). The SLM-produced TLM sample displays a microstructure with fine columnar grains having a direction with respect to the building direction and a strong texture aligned along the <001> direction (i.e. building direction) with a columnar shape. Such a texture has been extensively reported in different alloy systems and is mainly affected by the heat flow direction and gradient temperature during laser processing [25]. The columnar grains have an average width of ~30 μm and length of more than 1000 μm. The high density of sub-grains and low-angle sub-grain boundaries are evenly distributed in the β columnar grains. The low-angle sub-grain boundaries consisting of dislocation entanglement are related to thermal stress caused by rapid cooling in SLM process [15,18]. By contrast, the hot-rolled sample presents a microstructure comprising coarse equiaxed grains with the average size of ~200 μm. No sub-grains or sub-grain boundaries are observed in the single β-Ti equiaxed grains, and the uniform grain orientation is evident in the IPF result for hot-rolled TLM sample (Fig. 1b). Fig. 1c compares the typical XRD patterns for the TLM powder, SLM-produced and hot-rolled samples. All the samples mainly consist of a single body-centered cubic (bcc) β-Ti phase. Fig. 1d shows the hardness value at the points 1–6 in the SLM-produced (Fig. 1a) and hot-rolled TLM samples (Fig. 1b). The hardness values near the melt pool boundaries (223–230 HV) are higher than that in the melt pool core region (202 HV) of SLM-produced sample, while the hot-rolled sample presents a uniform hardness distribution.

Fig. 2a shows the typical tensile stress-strain curves for the SLM-produced and hot-rolled samples. Although both SLM-produced and hot-rolled TLM samples have the same constituent phase, they exhibit very different tensile mechanical behavior. The SLM-produced TLM sample has an ultimate tensile strength (UTS) of ~716±14 MPa and a ductility of ~37±5%, while the hot-rolled sample exhibits a lower UTS of

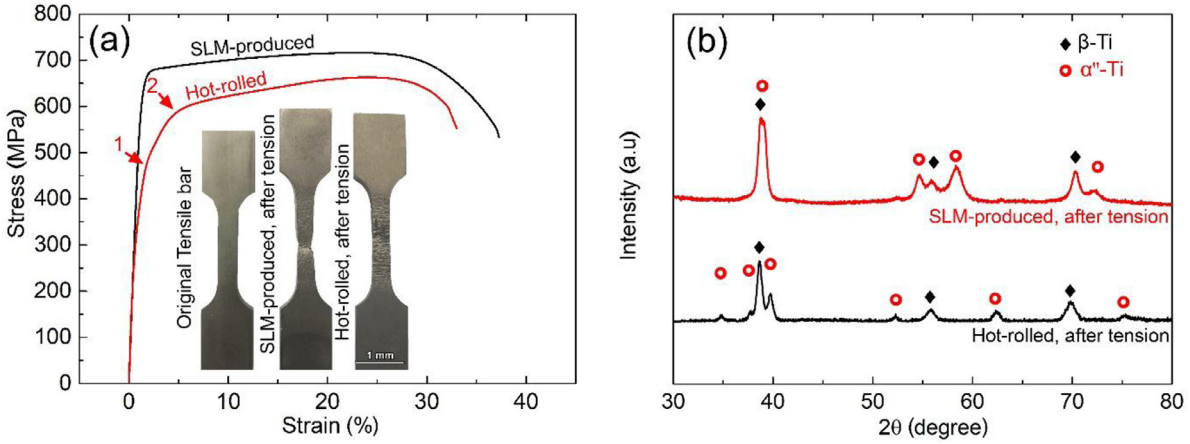

Fig. 2. (a) The typical tensile stress-strain curves for SLM-produced and hot-rolled TLM samples. The inset shows the tensile bars before and after tests, where the SLM-produced sample exhibits a good strength and ductility with an apparent necking effect. (b) XRD patterns of SLM-produced and hot-rolled samples after tensile tests. Both samples present a TRIP effect (i.e. the β to α'' phase transformation).

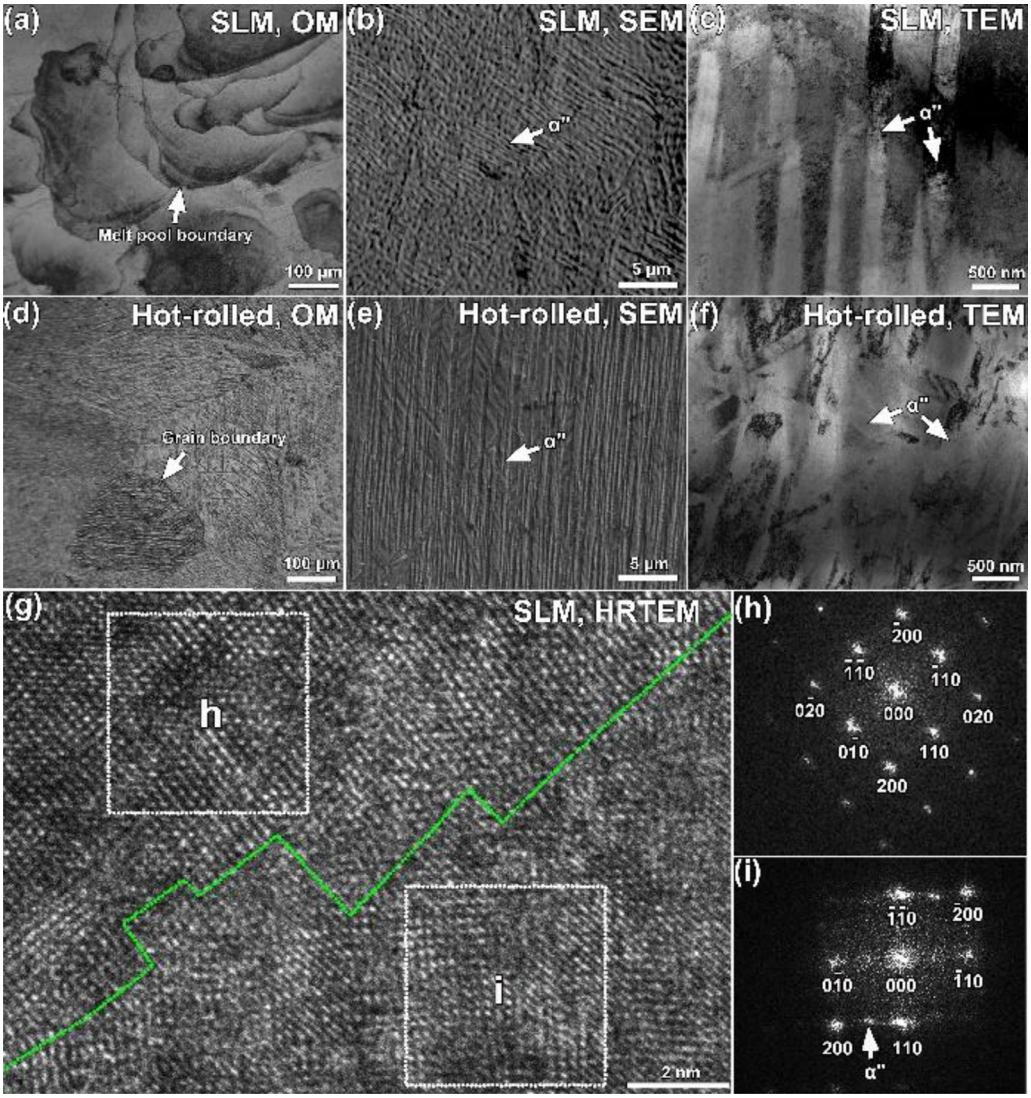

Fig. 3. The microstructural features of (a)–(c) SLM-produced and (d)–(f) hot-rolled TLM samples after tensile tests. OM: optical microscopy; SEM: scanning electron microscopy; TEM: transmission electron microscopy. (g) an HRTEM image of lath martensite plates in SLM-produced sample and the corresponding FFT diffraction patterns in (h) "h" and (i) "i" areas indicated in (g).

~622±21 MPa and a slightly lower ductility of ~32±4%. A prominent necking effect is observed near the fracture region of the SLM-produced TLM tensile bar, but the scenario is not noted for the hot-rolled counterpart (Fig. 2a inset). Apparently, the hot-rolled sample exhibits double yielding effect (where the two yield points are arrowed by "1" and "2" in Fig. 2a), while the SLM-produced TLM sample shows only one yielding point. The SLM-produced TLM sample exhibits a much higher yield strength (~592±21 MPa) compared with the hot-rolled TLM counterpart (~308±13 MPa). It is well known that the martensitic transformation-induced plasticity (TRIP effect, $\beta \rightarrow \alpha$") effect can reduce local stress concentration, delay crack formation and prevent crack propagation, thereby improving the ductility of titanium alloys during plastic deformation [24,26-29]. The previous study reported that the hot-rolled TLM samples presented large ductility during tensile testing due to the generation of lath martensite α" [24]. The XRD observations on tensile tested samples near the fracture region indicate that the martensitic transformation can be triggered for both SLM-produced and hot-rolled samples (Fig. 2b). The high yield strength with only one yielding point in SLM-produced samples should be caused by the generation of fine columnar grains and sub-grain boundaries. Previous studies revealed that the nucleation of martensite is sensitive to the grain size; the smaller the size of grains, the later the nucleation of the martensite phase [30,31]. Moreover, the martensitic transformation is sensitive to the orientation of the metal sample [32]; a strong textured polycrystalline usually lead to strain-induced martensitic transformation caused. The SLM-produced sample contains strong texture, high density of fine columnar grains and sub-grain boundaries, which would impede the martensitic transformation nucleation. Such the delayed TRIP effects can result in a higher yield strength in the SLM-produced TLM samples.

Fig. 3 illustrates the microstructural characteristics of SLM-produced and hot-rolled TLM samples after tensile testing. It is hard to find the lath martensite plates in the SLM-produced sample in OM image (Fig. 3a), where only the melt pool boundaries are apparent. By contrast, lath martensite plates are evident in OM image for the hot-rolled counterpart (Fig. 3d) and the size of most martensite plates reaches the full length of β grains. In SEM and TEM images, the lath martensite can be found inside β grains for both samples. Due to the occurrence of sub-grains and low-angle sub-grain boundaries, the length of lath martensite in SLM-produced TLM samples (Fig. 3b) is much shorter in size than that in the hot-rolled sample (Fig. 3e). For the hot-rolled sample, in the early stage of plastic deformation, the initially nucleated lath martensite α" plates would grow to the whole β grains, which produces considerable strain increments [33]. However, due to the presence of fine columnar β grains and sub-grains, the growth path of lath martensite α" plates in the SLM-produced sample are deflected and hard to extend to the whole β grains. During plastic deformation in tensile testing, the deformation bands start to form in the beginning of plastic deformation process.

Fig. 3g shows a TEM micrograph near the fracture surface of a SLM-produced TLM sample, illustrating the strain-induced martensite α" phase. The "h" region contains the single β phase (Fig. 3h) and the formation of strain-induced α" phase can be identified by the fast Fourier transform (FTT) diffraction pattern in Fig. 3i. The presence of lath martensite α" phase is also showed in XRD patterns (Fig. 2b). Sun et al. [34] stated that most lath martensite α" plates in β grains are formed from a one-step direct mechanism, i.e. $\beta \rightarrow \alpha$", while the remaining plates are produced through a two-step mechanism, i.e. $\beta_{matrix} \rightarrow \beta_{twinned} \rightarrow \alpha$". In this work, only the process of $\beta \rightarrow \alpha$" is observed, but the twinning effect is not detected in the TEM specimen. Thus, it can confirm that the good ductility of SLM-produced sample should be significantly affected by the strain-induced TRIP effect. Furthermore, the ductility of TLM sample could also be affected by the "hard-wraps-soft" structure; such a unique structure is formed in the laser melting process [23]. The higher hardness of the region near melt pool boundaries (223–230 HV) than that of the melt pool core region (202 HV) in SLM-produced TLM samples is ascribed to easy formation of ultra-fine grains or sub-grain boundaries near melt pool boundaries (Fig. 1d); such a phenomenon is called the "hard-wraps-soft" structure [23]. During plastic deformation, due to their different flow stresses at yielding point, the flow stress is higher in the hard region than in the soft region. As such, plastic deformation is still undertaken by the soft region, and the mismatch dislocations would account for the plasticity mismatch. As the strain increases, the geometrically necessary dislocations would increase because of the difference in flow stress between the hard and soft regions. Therefore, the back stress in the "hard-wraps-soft" structure increases with the strain. As such, combined with the strain-induced TRIP effect and "hard-wraps-soft" effect, the SLM-produced TLM sample exhibits good tensile ductility. Fig. 4 shows the tensile fracture surface of the SLM-produced and hot-rolled samples. Although dimples are prominent in both samples, the SLM-produced sample has more dimples and the dimple size is finer compared to the hot-rolled sample, which results from the finer grains and the sub-grain generation in SLM-produced sample. The fractographical results reveal that the ductility in the SLM-produced sample, with

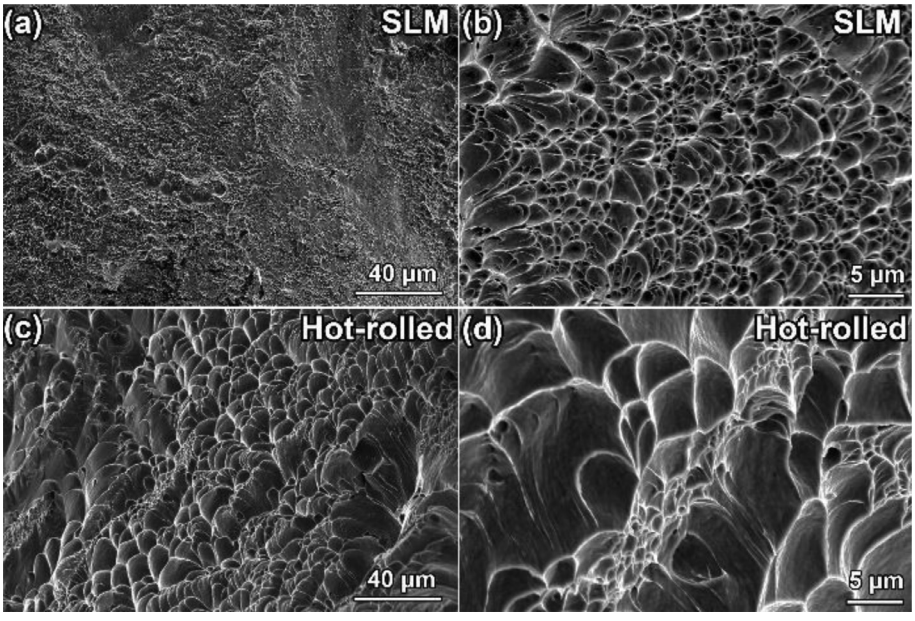

Fig. 4. The tensile fracture surface of the (a) and (b) SLM-produced and (c) and (d) hot-rolled TLM samples. The size of the dimple in SLM-produced sample is more and finer than that of the hot-rolled counterparts.

finer grain size and hence more dimples generation, is greater than that of the hot-rolled sample [35].

In summary, the microstructures, yield strength, ultimate tensile strengths and ductility of the selective laser melting produced (SLM-produced) and hot-rolled β-type TLM (Ti-25Nb-3Zr-3Mo-2Sn) parts have been systematically compared. The SLM-produced TLM part consists of the unique microstructure in terms of strong texture, the strain-induced martensitic transformation and "hard-wraps-soft" structure, which makes the SLM-produced TLM part more ductile than the conventional hot-rolled counterpart. Simultaneously, both the yield strength and ultimate tensile strength are increased, which are attributed to the formation of fine columnar grains, sub-grains and sub-grain boundaries. The excellent combination of mechanical properties (simultaneously high strength and large ductility) of SLM-produced metastable β titanium part would shed insight into future applications in biomedical field.

Declaration of interests

The authors declare that they have no known competing financial interests or personal relationships that could have appeared to influence the work reported in this paper. The authors declare the following financial interests/personal relationships which may be considered as potential competing interests.

Acknowledgment

This work was supported partially by Australian Research Council Discovery Project (DP110101653) and Innovation Team in Key Areas of Shaanxi Province (2016KCT-30).

References

[1] M. Long, H.J. Rack, Titanium alloys in total joint replacement-a materials science perspective, Biomaterials 19 (1998) 1621–1639.
[2] L.C. Zhang, Y. Liu, S. Li, Y. Hao, Additive manufacturing of titanium alloys by electron beam melting: a review, Adv. Eng. Mater. 20 (2018) 1700842.
[3] N. Dai, L.C. Zhang, J. Zhang, Q. Chen, M. Wu, Corrosion behavior of selective laser melted Ti-6Al-4 V alloy in NaCl solution, Corros. Sci. 102 (2016) 484–489.
[4] P. Qin, Y. Liu, T. Sercombe, Y. Li, C. Zhang, C. Cao, H. Sun, L.C. Zhang, Improved corrosion resistance on selective laser melting produced Ti-5Cu alloy after heat treatment, ACS Biomater. Sci. Eng. 4 (2018) 2633–2642.
[5] C. Rabadia, Y. Liu, L. Wang, H. Sun, L.C. Zhang, Laves phase precipitation in Ti-Zr-Fe-Cr alloys with high strength and large plasticity, Mater. Des. 154 (2018) 228–238.
[6] L.C. Zhang, D. Klemm, J. Eckert, Y. Hao, T. Sercombe, Manufacture by selective laser melting and mechanical behavior of a biomedical Ti-24Nb-4Zr-8Sn alloy, Scr. Mater. 65 (2011) 21–24.
[7] Y. Liu, J.S. Li, H. Wang, W. Hou, Y. Hao, R. Yang, T. Sercombe, L.C. Zhang, Microstructure, defects and mechanical behavior of beta-type titanium porous structures manufactured by electron beam melting and selective laser melting, Acta Mater. 113 (2016) 56–67.
[8] Y. Liu, H. Wang, S. Li, S. Wang, W. Wang, W. Hou, Y. Hao, R. Yang, L.C. Zhang, Compressive and fatigue behavior of beta-type titanium porous structures fabricated by electron beam melting, Acta Mater. 126 (2017) 58–66.
[9] P. Qin, Y. Chen, Y. Liu, J. Zhang, L. Chen, Y. Li, X. Zhang, C. Cao, H. Sun, L.C. Zhang, Resemblance in corrosion behavior of selective laser melted and traditional monolithic β Ti-24Nb-4Zr-8Sn alloy, ACS Biomater. Sci. Eng. 5 (2019) 1141–1149.
[10] Y.J. Liu, X.P. Li, L.C. Zhang, T.B. Sercombe, Processing and properties of topologically optimised biomedical Ti-24Nb-4Zr-8Sn scaffolds manufactured by selective laser melting, Mater. Sci. Eng. A 642 (2015) 268–278.
[11] Y.J. Liu, S.J. Li, L.C. Zhang, Y.L. Hao, T.B. Sercombe, Early plastic deformation behaviour and energy absorption in porous β-type biomedical titanium produced by selective laser melting, Scr. Mater. 153 (2018) 99–103.
[12] N. Hafeez, S. Liu, E. Lu, L. Wang, R. Liu, L.C. Zhang, Mechanical behavior and phase transformation of β-type Ti-35Nb-2Ta-3Zr alloy fabricated by 3D-Printing, J. Alloys Compd. 790 (2019) 117–126.
[13] S. Hao, L. Cui, D. Jiang, X. Han, Y. Ren, J. Jiang, Y. Liu, Z. Liu, S. Mao, Y. Wang, A transforming metal nanocomposite with large elastic strain, low modulus, and high strength, Science 339 (2013) 1191–1194.
[14] Y. Liu, Z. Liu, Y. Jiang, G. Wang, Y. Yang, L.C. Zhang, Gradient in microstructure and mechanical property of selective laser melted AlSi10Mg, J. Alloys Compd. 735 (2018) 1414–1421.
[15] X. Lei, L. Dong, Z. Zhang, Y. Liu, Y. Hao, R. Yang, L.C. Zhang, Texture evolution and mechanical properties of VT3-1 titanium alloy processed by multi-pass drawing and subsequent isothermal annealing, Metals 7 (2017) 131.
[16] K. Lu, Stabilizing nanostructures in metals using grain and twin boundary architectures, Nat. Rev. Mater. 1 (2016) 16019.
[17] L. Wang, L. Xie, Y. Lv, L.-C. Zhang, L. Chen, Q. Meng, J. Qu, D. Zhang, W. Lu, Microstructure evolution and superelastic behavior in Ti-35Nb-2Ta-3Zr alloy processed by friction stir processing, Acta Mater. 131 (2017) 499–510.
[18] K. Lu, L. Lu, S. Suresh, Strengthening materials by engineering coherent internal boundaries at the nanoscale, Science 324 (2009) 349–352.
[19] Y. Lu, W. Lin, M. Xie, W. Xu, Y. Liu, J. Lin, C. Yu, K. Tang, W. Liu, K. Yang, Examining Cu content contribution to changes in oxide layer formed on selective-laser-melted CoCrW alloys, Appl. Surf. Sci. 464 (2019) 262–272.
[20] Y.J. Liu, S.J. Li, W.T. Hou, S.G. Wang, Y.L. Hao, R. Yang, T. Sercombe, L.C. Zhang, Electron beam melted beta-type Ti-24Nb-4Zr-8Sn porous structures with high strength-to-modulus ratio, J. Mater. Sci. Technol. 32 (2016) 505–508.
[21] J. Hernandez, S.J. Li, E. Martinez, L.E. Murr, X.M. Pan, K.N. Amato, X.Y. Cheng, F. Yang, C.A. Terrazas, S.M. Gaytan, Microstructures and Hardness Properties for β-Phase Ti-24Nb-4Zr-7.9 Sn Alloy Fabricated by Electron Beam Melting, J. Mater. Sci. Technol. 29 (2013) 1011–1017.
[22] B. Vrancken, L. Thijs, J.-P. Kruth, J. Van Humbeeck, Microstructure and mechanical properties of a novel β titanium metallic composite by selective laser melting, Acta Mater 68 (2014) 150–158.
[23] C. Yang, Z. Zhang, S. Li, Y. Liu, T. Sercombe, W. Hou, P. Zhang, Y. Zhu, Y. Hao, Z. Zhang, Simultaneous improvement in strength and plasticity of Ti-24Nb-4Zr-8Sn manufactured by selective laser melting, Mater Des. 157 (2018) 52–59.
[24] Y. Zhentao, Z. Lian, Influence of martensitic transformation on mechanical compatibility of biomedical β type titanium alloy TLM, Mater. Sci. Eng. A 438 (2006) 391–394.
[25] G.P. Dinda, A.K. Dasgupta, J. Mazumder, Texture control during laser deposition of nickel-based superalloy, Scr. Mater. 67 (2012) 503–506.
[26] M. Marteleur, F. Sun, T. Gloriant, P. Vermaut, P.J. Jacques, F. Prima, On the design of new β-metastable titanium alloys with improved work hardening rate thanks to simultaneous TRIP and TWIP effects, Scr. Mater. 66 (2012) 749–752.
[27] J. Zhang, S. Hao, D. Jiang, Y. Huan, L. Cui, Y. Liu, Y. Ren, H. Yang, Dual phase synergy enabled large elastic strains of nanoinclusions in a dislocation slip matrix composite, Nano Lett. 18 (2018) 2976–2983.
[28] J. Zhang, Y. Liu, Y. Ren, Y. Huan, S. Hao, C. Yu, Y. Shao, Y. Ru, D. Jiang, L. Cui, In situ synchrotron X-ray diffraction study of deformation behavior and load transfer in a Ti2Ni-NiTi composite, Appl. Phys. Lett. 105 (2014) 041910.
[29] F. Fischer, Q.P. Sun, K. Tanaka, Transformation-induced plasticity (TRIP), Appl. Mech. Rev. 49 (1996) 317–364.
[30] J. Zhang, S. Hao, D. Jiang, Y. Huan, L. Cui, Y. Liu, H. Yang, Y. Ren, In situ synchrotron high-energy X-ray diffraction study of microscopic deformation behavior of a hard–soft dual phase composite containing phase transforming matrix, Acta Mater. 130 (2017) 297–309.
[31] X. Shi, F. Guo, J. Zhang, H. Ding, L. Cui, Grain size effect on stress hysteresis of nanocrystalline NiTi alloys, J. Alloys Compd. 688 (2016) 62–68.
[32] K. Gall, T.J. Lim, D.L. McDowell, H. Sehitoglu, Y.I. Chumlyakov, The role of intergranular constraint on the stress-induced martensitic transformation in textured polycrystalline NiTi, Int. J. Plast. 16 (2000) 1189–1214.
[33] T. Grosdidier, M.-J. Philippe, Deformation induced martensite and superelasticity in a β-metastable titanium alloy, Mater. Sci. Eng. A 291 (2000) 218–223.
[34] F. Sun, J. Zhang, M. Marteleur, C. Brozek, E. Rauch, M. Veron, P. Vermaut, P. Jacques, F. Prima, A new titanium alloy with a combination of high strength, high strain hardening and improved ductility, Scr. Mater. 94 (2015) 17–20.
[35] S. Ehtemam-Haghighi, Y. Liu, G. Cao, L.C. Zhang, Phase transition, microstructural evolution and mechanical properties of Ti-Nb-Fe alloys induced by Fe addition, Mater. Des. 97 (2016) 279–286.